SLAC-PUB-12001
August 2006

SUPPRESSION OF SECONDARY EMISSION IN A MAGNETIC FIELD USING A SAWTOOTH AND ISOSCELES TRIANGLE SURFACE

L. Wang, T. Raubenheimer and G. Stupakov, SLAC, Menlo Park, CA, USA

Abstract

The effect of surface roughness on the secondary electron emission from a sawtooth and isosceles triangle surface in a magnetic field under electron bombardment is investigated using a Monte-Carlo method. Some of the secondary electrons emitted from the surface return to the surface within their first few gyrations, resulting in a low effective secondary electron yield. Both sawtooth and isosceles triangle surface in magnetic field can significantly reduce the secondary emission yield below the multipacting threshold with weak dependence on the size of surface and megnetic field.

Presented at Vancouver Linear Collider Workshop
19-22 July 2006, Vancouver, Canada

Submitted to Nuclear Instruments and Methods in Physics Research Section A

Work supported in part by Department of Energy contract DE-AC02-76SF00515

SUPPRESSION OF SECONDARY EMISSION IN A MAGNETIC FIELD USING A SAWTOOTH AND ISOSCELES TRIANGLE SURFACE*

L. Wang#, T. Raubenheimer and G. Stupakov, SLAC, Menlo Park, CA, USA

Abstract

The effect of surface roughness on the secondary electron emission from a sawtooth and isosceles triangle surface in a magnetic field under electron bombardment is investigated using a Monte-Carlo method. Some of the secondary electrons emitted from the surface return to the surface within their first few gyrations, resulting in a low effective secondary electron yield. Both sawtooth and isosceles triangle surface in magnetic field can significantly reduce the secondary emission yield below the multipacting threshold with weak dependence on the size of surface and magnetic field.

Keywords: Electron cloud instability; Secondary electron yield; magnetic field; Monte Carlo; grooved surface; sawtooth surface; isosceles triangle surface

INTRODUCTION

Electron cloud due to multipacting can cause transverse beam instabilities, beam loss, vacuum pressure rise, transverse beam size increase and heat load deposited on the chamber wall due to the lost electrons. Multipacting is induced by beam itself. Electrons gain energy from the beam. Therefore, multipacting happens in high intensity rings where electrons can gain sufficient energy for multipacting. Electron clouds have been observed in almost all the recent intensity proton/positron rings, such as the Proton Storage Ring at Los Alamos National Laboratory (LANL-PSR), Spallation Neutron Source (SNS) at Oak Ridge National Laboratory (ORNL), B-factory at High Energy Accelerator Research Organization (KEK) and Stanford Linear Accelerator Center (SLAC), European Organization for Nuclear Research's Proton Synchrotron (PS) and Super Proton Synchrotron (SPS), Relativistic Heavy Ion Collider (RHIC) and Alternating Gradient Synchrotron (AGS) at Brookhaven National Laboratory (BNL) [1].

A weak solenoid is a good remedy to suppress the electron multipacting in a drift region by confining the electrons near the pipe surface[2, 3, 4]. However, it doesn't work in a magnet where strong multipacting can happen. The electron cloud from dipole magnets and wigglers in the positron damping ring of the International Linear Collider(ILC) gives a critical limitation on the choice of a circumference of the damping ring, which directly results in a choice of two 6km rings as the baseline for the positron damping ring. Clearing electrodes may work as a possible remedy. A tradition stripline type electrode has been proposed for LHC[5]. Simulation shows that a wire type electrode works perfectly in all types of magnets [6]. In practice, the secondary emission yield (SEY) can be reduced by coating of the metal surface[7-13], surface cleaning[14] and beam scrubbing[15, 16]. Surface roughness is another type of remedy to reduce the SEY. The surface roughness effect on the secondary emission in field free case has been studied [8, 17-21]. A triangular grooved surface in field free region reduces the peak SEY of aluminum from 3.2 to 2.4 [8]. A sawtooth surface in field free region is effective to reduce the electron emission under the situation without strong beam fields where the electron multipacting hardly occurs [21]. A dipole magnetic field attenuates the photoelectron emission from the surface by more than two orders of magnitude with the magnetic field aligned parallel to the surface [22]. A rectangular grooved surface in field free region of PEPII is under study[23]. A similar study is planned at KEKB [24].

Three types of surface has been investigated in this paper: sawtooth, isosceles triangle and rectangular surface. To simulate the secondary electrons' emission from the surface we apply a Monte Carlo program CLOUDLAND, which includes the detail model of electron-surface interaction and electron motion in magnetic field. Program CLOUDLAND is a 3D particle in cell code for the simulation of electron multipacting with various charged beam, electric and magnetic fields. Simulation shows that both sawtooth and isosceles triangular surface in a magnetic field can significantly reduce the SEY by restricting the secondary electrons near the surface.

MONTE CARLO SIMULATION

The basic idea of the Monte-Carlo model of secondary electron emission used here is to simulate trajectories of primary and secondary electrons in a electric or magnetic field. When the primary electrons interact with a surface, secondary electrons are generated using a series of random numbers to determine their energy and velocity according to given secondary emission parameters.

According to Furman [25], Seiler [26] and Kirby [27], the yield of the true secondary emission can be written as

$$\delta_{Y_{ts}}(E,\theta) = \delta_{\max} 1.11 x^{-0.35}(1 - e^{-2.3x^{1.35}}) \exp(0.5(1-\cos\theta)) \quad (1)$$

where, $x = E_p(1+0.7(1-\cos\theta))/E_{\max}$, E_p is primary electron energy, E_{max} is the energy of the maximum

*Work supported by the U.S. Department of Energy under contract DE-AC03-76SF00515

electric address: wanglf@slac.stanford.edu

secondary emission yield, δ_{max} the maximum secondary emission yield for perpendicular incidence, θ is the incidence angle with respect to the surface normal. Besides true secondary electrons, backscattered electrons and rediffused electrons are also emitted when electrons hit the surface. The detail model of secondary electron emission of CLOUDLAND is described in [28, 29]. Two series of secondary parameters are considered here: δ_{max}=1.40, E_{max}=190 *eV* and δ_{max}=1.74, E_{max}=330eV.

The initial energy distribution of the true secondary emission is taken to be a half-Gaussian centered at zero with an rms (root mean square) spread of 5 *eV*.

$$\delta_E(E_{st}) = \delta_{E\_st}\exp\left(-E_{st}/2\delta^2_{E\_st}\right)_{Est>0} \quad (2)$$

The angular distribution of the trajectories of the secondary electrons as they emerge from the surface is described by a cosine function:

$$\chi(\phi) = \chi_0 \cos\phi \quad (3)$$

Where ϕ is the angle between the surface normal and the direction of the measurement, and χ_0 is the value of χ along the surface normal. This cosine distribution is rotationally symmetric about the surface normal. The effective SEY is calculated by the ratio of electrons coming out from the surface to the primary electrons. In each step, the secondary electrons are generated by 10^5 primary electrons.

The electron multipacting in magnetic fields usually happens at the location where the field lines are perpendicular to the surface. For example, inside dipole magnets, two stripes of multipacting occurs near the middle of horizontal coordinate [28, 30]. Multipacting in quadrupole magnet occurs at the middle of the magnetic poles. Therefore, a dipole magnetic field which is perpendicular to the surface is assumed in this paper. The results of this paper apply straight to quadrupole magnet and others. In this paper, we assume a dipole magnetic field of 0.2 Tesla and 1.6 Tesla, which is dipole magnet field and wiggler field in the ILC damping ring. The dipole magnetic field of B-factories is 0.3 Tesla. The gyration radius of an electron in magnetic field B_0 is

$$r_0 = \gamma m_0 \upsilon / eB_0 \quad (4)$$

where *e* and m_0 are the charge and mass of the electron. υ is velocity of the electron. r_0=37.7μm, 0.23*mm* and 0.31*mm* for an electron with energy 5eV, 190eV and 330*eV* in a 0.2 Tesla field, respectively. r_0=4.7μm, 28μm and 39μm for an electron with energy 5eV, 190eV and 330eV in a 1.6 Tesla field, respectively.

CAPTURE OF SECONDARY ELECTRONS

The suppression mechanism of the secondary electrons' emission is to confine the secondary electrons near the wall surface by the magnetic field. In a dipole magnet, B=(0, B_0, 0), the trajectory of a secondary electron is a helix:

$$\begin{cases} x = x_0 + \dfrac{\upsilon_{x0}}{\omega_0}\sin\omega_0 t - \dfrac{\upsilon_{z0}}{\omega_0}\left(\cos\omega_0 t - 1\right) \\ z = z_0 + \dfrac{\upsilon_{z0}}{\omega_0}\sin\omega_0 t + \dfrac{\upsilon_{x0}}{\omega_0}\left(\cos\omega_0 t - 1\right) \\ y = y_0 + \upsilon_{y0} t \end{cases} \quad (5)$$

Where the subscript index 0 means the emission parameters of the secondary electron emitted from a tilted surface with a slope angle α as shown in Fig. 1. $\omega_0 = eB_0/m_0\gamma$ is the gyration frequency in the magnetic field.

A secondary electron emitted from the tilted surface runs into the surface when its trajectory intersects with the surface:

$$\zeta = \frac{\upsilon_{y0}}{\upsilon_{\perp 0}}\omega_0 t \cdot ctg\alpha - \sin\left(\omega_0 t + \Psi\right) - \frac{\upsilon_{z0}}{\upsilon_{\perp 0}} \le 0,\ t \ge 0 \cdot \quad (6)$$

where $\Psi = Arc\sin(\upsilon_{z0}/\upsilon_{\perp})$ and $\upsilon_{\perp 0} = \left(\upsilon_{x0}^2 + \upsilon_{z0}^2\right)^{1/2}$ is the gyration motion (transverse) velocity. The secondary electron hits the plane if $\zeta \le 0$ at a certain time $t \ge 0$.

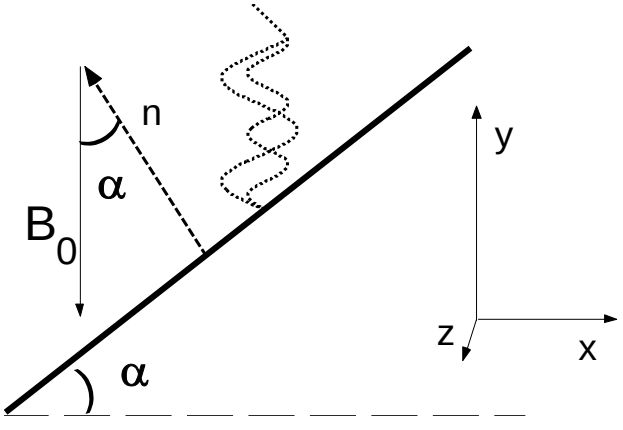

Fig. 1 Scheme of the trajectory of secondary electron emitted from a tilted surface in a magnetic field.

From Eq.(6), we can get the characters of capture probability of secondary electrons from a large tilted surface:

Magnetic field independent

From Eq. (6), the function ζ depends $\omega_0 t$, where *t* is a variable. Therefore, whether a secondary electron can hit the plane doesn't depends on the magnetic field B_0. Magnetic field can only change the time of the electron colliding with the surface.

Energy independent

For a certain tilted surface (fixed α), the probability of a secondary hitting the tilted surface depends on the angular distribution of secondary electrons ($\upsilon_{y0}/\upsilon_{\perp 0}$ and $\upsilon_{z0}/\upsilon_{\perp 0}$) only, instead of its energy. Note that SEY depends on the energy of the incident electrons.

Emission angle/α dependent

The angular distribution of the secondary electrons doesn't depend on the incident angle of the primary electrons. It remains a cosine distribution even for a tilted surface (Eq.3). Therefore, the angular distribution depends on only the slope angle of the surface. Therefore, the capture probability of secondary electrons is a function of α only. Note that α is the angle between the surface normal and the direction of the magnetic field lines (vertical here).

From Eq. (6), we can conclude that if $\upsilon_{y0}<0$, the secondary electron can be captured. The probability of $\upsilon_{y0}<0$ increases with α and has a maximum 50% when $\alpha=90^0$.

For a $\upsilon_{y0}>0$, the first term of ζ decreases with α. The function $ctg\alpha$ approximately linear decreases with α when $\alpha>70^0$ and it is 0.35 at 70^0 and 0 at 90^0. While the second and third term of ζ have a maximum of 1.0. Therefore, the probability of a secondary returning the surface increases quickly at large α. Fig. 2 shows the function ζ with $\alpha=40^0$ and $\alpha=70^0$. The probability of $\zeta \le 0$ with $\alpha=70^0$ is much larger that that with $\alpha=40^0$.

Fig. 3 shows the capture probability of secondary electrons from the tilted surface with different α. The line with legend δ(0) shows the probability of a secondary running into the surface (Eq. (6)). When the secondary electrons hit the surface, they may generate tertiary electrons with a small electron yield due to reflection and other mechanisms. The SEY due to the secondary electrons' hitting is close to the SEY at zero energy δ(0). Assuming a constant δ(0) for all secondary electrons, the capture probability of secondary electrons due to multiple hitting of the surface can be roughly expressed as

$$P(\delta(0)) = P_0 - P_0 \frac{\delta(0)(1-P_0)}{1-\delta(0)P_0} \qquad (7)$$

Where P_0 is the probability of a secondary returning to the surface, which is the case of $\delta(0)=0$. The capture probability with $\delta(0)=0.1$, 0.3 and 0.6 are also shown in Fig. 3. $\delta(0)$ depends on the property of the surface material. In this paper $\delta(0)=0.3$ is assumed. The capture probability is small than 20% with $\alpha<50^0$. A slope angle $\alpha>70^0$ is required in order to capture 60% the secondary electrons. A title surface with $\alpha=80^0$ can capture 80% of the secondary electrons. When the surface is vertical ($\alpha=90^0$), it can capture 100% secondary electrons.

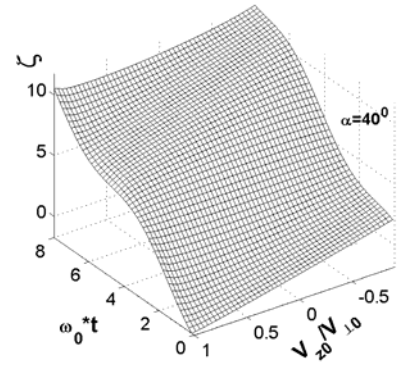

(a)

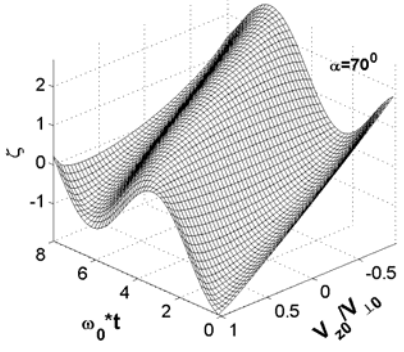

(b)

Fig. 2. Function ζ with different tilted surface $\alpha=40^0$ (a) and $\alpha=70^0$ (b). $\upsilon_{y0}/\upsilon_{\perp_0} = ctg\alpha$ (emitted at surface normal direction) is assumed.

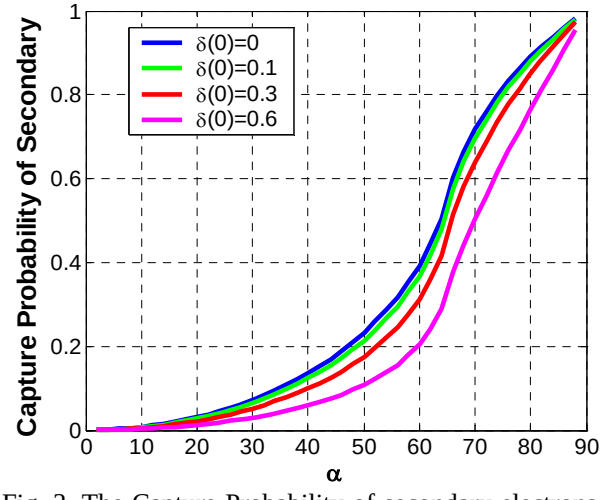

Fig. 3. The Capture Probability of secondary electrons in magnetic field from a tilted surface with slope angle α.

SAWTOOTH SURFACE

Fig. 4 shows the geometry of a sawtooth surface. Its surface is a sawtooth function

$$S(x) = h * frac(\frac{x}{W} + \vartheta), \qquad (8)$$

Where *frac* is the fractional part $frac(x) = x - \lfloor x \rfloor$, h is the height, W is the period of the surface, and ϑ is its phase. Its profile is a right triangle. The effect of sawtooth surface is a combined effect of two surfaces with $\alpha=90^0$ and $\alpha<90^0$.

The vertical edges parallel to the magnetic field lines. If an electron hits these edges, it makes a half circle like motion and then hits the surface again with a low SEY due to its low energy. The period of electron's gyration motion $2\pi m_0\gamma / eB$ is 0.179 ns in a 0.2 Tesla magnetic field, while the bunch spacing of ILC damping ring and B-factories ranges from 3 to 8ns. Therefore, the secondary electrons can hit the surface dozens times with small SEYs. In principle, these edges can completely suppress the secondary emission, which means the secondary electrons cannot go up and return to the beam chamber (Fig. 3). There is a similar mechanism to suppress the electrons using a weak solenoid in field free region.

The tilted edges with a slope angle of α cannot trap all the secondary electrons. Some secondary electrons make gyration motion and hit the surface several times, then go up. Parts of secondary electrons can directly go up and enter the beam chamber without any collision with the tilted edges. The effect of this surface strongly depends on the slope angle α (Fig. 3). The electrons' orbits in Fig. 4 clearly show the trapping mechanism.

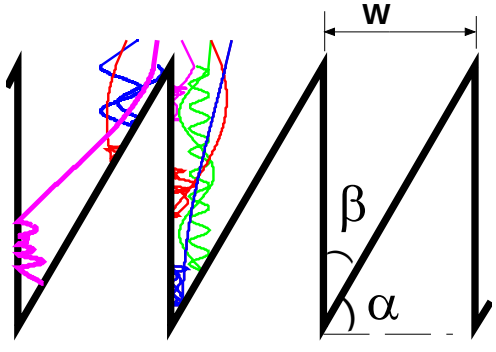

Fig. 4. Sawtooth surface ($\alpha + \beta = \pi/2$). The period is W and height is h. Orbits of electrons show the mechanism of confinement of secondary electrons.

Slope angle effect

The probability of secondary electrons hitting the tilted edge is sensitive to the slope angle α (Fig. 3). The larger the slope angle α, the bigger the probability. Fig. 5 shows the effective SEY from a sawtooth surface with α=0°(flat surface), 60°, 70° and W=0.28*mm* in a 0.2 Tesla magnetic field. The peak effective SEY with a flat surface is about 1.9, which is bigger than δ_{max}=1.40 due to the effect of grazing angle: the SEY is roughly proportional to $1/\cos(\theta)$. A sawtooth surface with α=60° reduces the peak effective SEY below 0.9. A surface with α=70° reduces it further with a peak SEY of 0.6. Therefore, for a surface material with δ_{max}=1.4, a sawtooth surface with α=60° and W=0.38*mm* is enough to suppress the electron multipacting.

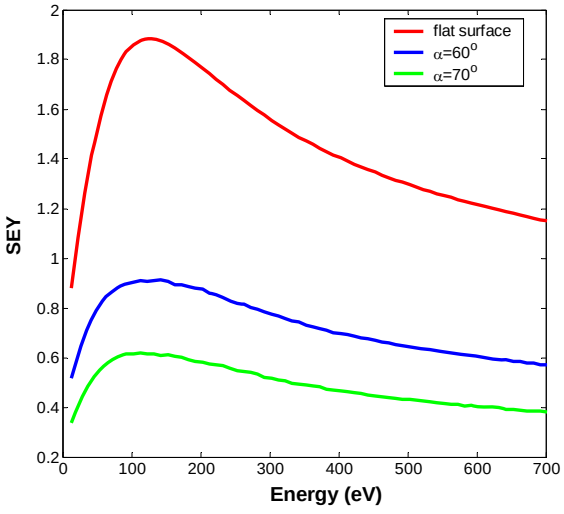

Fig. 5. Effective SEY from sawtooth surface in a dipole magnetic field. δ_{max}=1.40, E_{max}=190eV, B_0=0.2Tesla, W=0.38 *mm*.

Effect of W

Fig. 6 shows the effective SEY from the sawtooh surface with different W and α. The material of the surface has a δ_{max} of 1.74 at 330eV. The magnetic field is 0.2Tesla. The suppression effect of SEY from the surface is not monotonic. With a smaller W, the primary electrons cannot deeply enter the sawtooth surface due to their larger gyration motion radius comparing with W. Therefore, the secondary electrons have more probability to go up and enter to the beam chamber. If W is larger, the primary electrons have more chance to hit the tilted edges instead of the vertical edges. Note that the vertical edge has larger capture capability than the tilted one. Therefore, a surface with bigger W has bigger effective SEY. There is a minimum SEY when W is about the gyration motion radius at the energy with peak SEY, which is 0.306*mm*. The SEY gets saturated with further increment of W. With a large α, the effect of W becomes smaller as shown in Fig. 6. There are small effective SEYs (<0.76) when W ranges from 0.38*mm*~1.89*mm* with α=70°. The SEY gets saturated near W=1.89*mm*. A special case with δ_{max}=2.5, α=70° and W=0.38*mm* is also shown in Fig. 6. There is still no multipacting even with δ_{max}=2.5.

Magnetic field effect

Fig. 7 shows the effective SEY from the sawtooh surface in a 0.3 Tesla magnetic field. The SEY of the surface material is the same as Fig. 6. The comparison of Fig. 7 with Fig. 6 shows the effective SEY is the

same if $W * B_0$ is a constant, which indicts that the ratio of W to the gyration motion radius is the same. Therefore, a stronger magnetic field corresponds to a smaller W. Magnetic field doesn't make difference when W is very large comparing to the gyration motion radius.

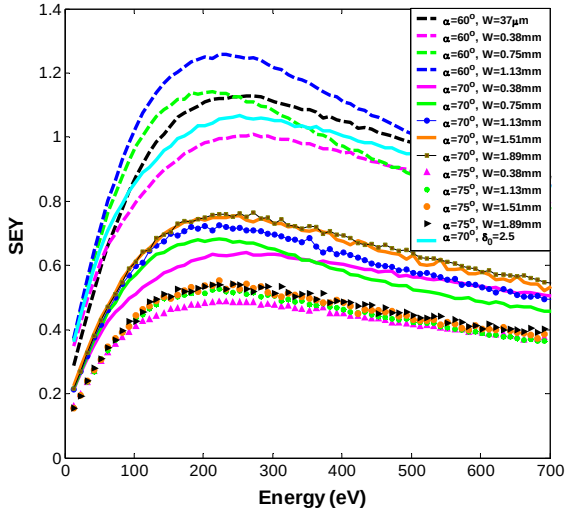

Fig. 6. Effective SEY from sawtooth surface in a dipole magnetic field. δ_{max}=1.74, E_{max}=330eV, B_0=0.2Tesla. A special case with δ_{max}=2.5, α=70° and W=0.38*mm* is also shown in the Figure.

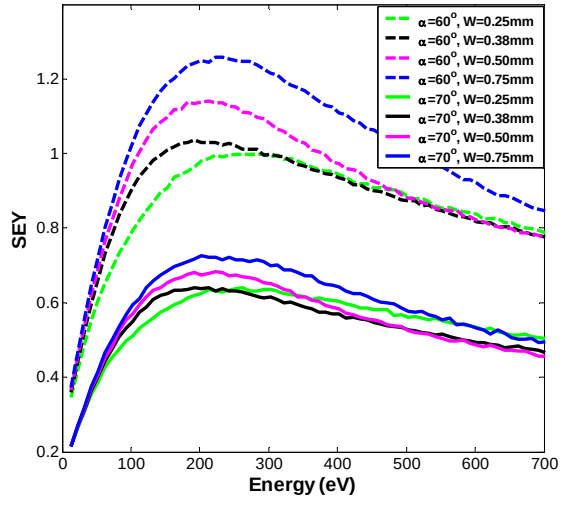

Fig. 7. Effective SEY from sawtooth surface in a dipole magnetic field. δ_{max}=1.74, E_{max}=330eV, B_0=0.3Tesla.

ISOSCELES TRIANGLE SURFACE

The geometry of an isosceles triangular surface is shown in Fig. 8. It consists of two tilted surfaces with a same slope angle. Its capture capability of secondary electrons is directly shown in Fig. 3. Fig. 9 shows the effective SEY of isosceles triangular surface with different W and α. The effective SEY is very sensitive to α, which agrees with the analytical result shown in Fig. 3. The SEY decreases from 1.3 to 0.4 when α increases from 65^0 to 80^0. The effective SEY has weak dependence on W. There is a bigger SEY at small W because some of the electrons cannot deeply enter the surface. It saturates at large W of 1.5 *mm* with the level of infinite large surface shown in Fig. 3. Note that the gyration motion radius of an electron with energy at peak SEY (330eV here) is 0.306*mm*. Similar as sawtooth surface, the property of SEY saturation at large W offers us more opportunity on the choice of the size of groove surface. A large size surface is easy to be manufactured.

Fig. 10 shows the effective SEY from an isosceles triangular surface with different α in a 1.6 Tesla field. A constant W=1.89*mm* is used here. Comparison of Fig. 9 with Fig. 10 shows that the effect of magnetic field is negligible at the large W.

Both sawtooth and isosceles triangle surface can significantly reduce the effective SEY with a weak dependence on the size of surface and magnetic field. With the same α, sawtooth surface is more effective. Isosceles triangle surface has smaller SEY than sawtooth surface for the same β when $\alpha > 50^0$.

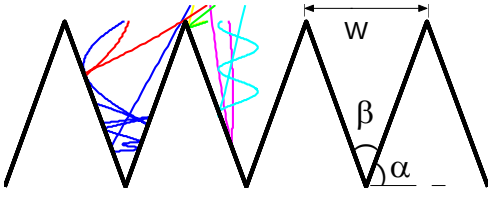

Fig. 8. Isosceles triangular surface ($\alpha + \beta/2 = \pi/2$).

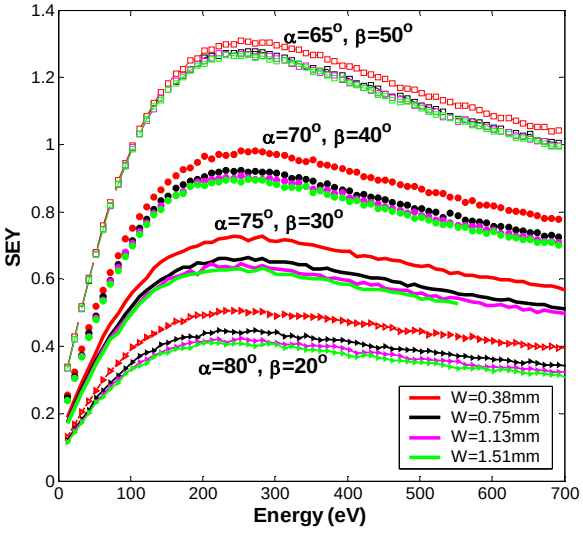

Fig. 9. Effective SEY from an isosceles triangular surface with α=65°, 70°, 75°, and 80° in a dipole magnetic field. For each α, the SEYs with W=0.38*mm*, 0.75*mm*, 1.13*mm* and 1.51*mm* are calculated. δ_{max}=1.74, E_{max}=330eV, B_0=0.2Tesla.

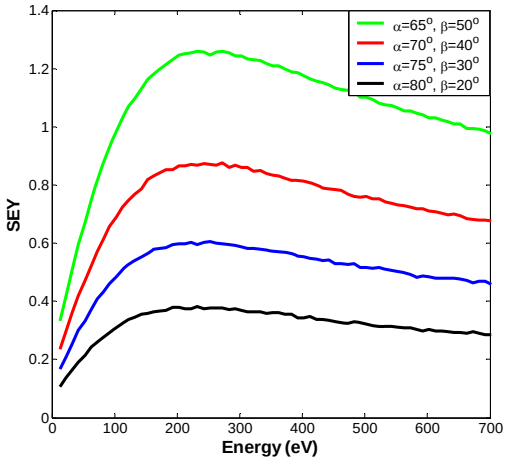

Fig. 10. Effective SEY from an isosceles triangular surface in a dipole magnetic field. δ_{max}=1.74, E_{max}=330eV, B_0=1.6Tesla and W=1.89*mm*.

RECTANGULAR SURFACE

Rectangular surface is another simple surface. Fig. 11 shows the geometry of a rectangular surface. Rectangular surface consists of two types of edges: α=90° and α=0°. In principle, the two special edges can capture 100% and 0% secondary electrons, respectively, as shown in Fig. 3. The probability of an electron hitting the vertical and flat edge depends on *b*, the width of the groove, and the radius of gyration motion. Therefore, the effective SEY of a rectangular surface in a magnet field is sensitive to the size of the surface and the magnetic field.

Fig. 12 shows the effective SEY of rectangular surface with different size in a 0.2 Tesla magnetic field. A very small shoulder width *a* is assumed in order to investigate the effect of *b*. The effect of *b* is not monotonic. The electrons cannot deeply enter the grooved surface with a small *b*. On the other hand, if *b* is too big comparing with the radius of gyration motion near E_{max}, more electrons hit the bottom flat surface, which cannot trap any secondary electrons. To reduce the SEY below 1.0, *W* should range from 0.08*mm* to 0.51*mm* as shown in Fig. 12. A smaller size *W* is required in a 1.6 Tesla magnetic field as shown in Fig. 13. The required *W* ranges from 21μm to 63 μm.

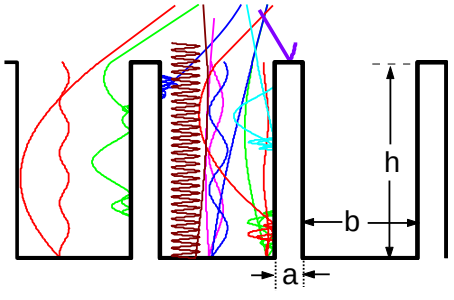

Fig. 11. Rectangular surface. Period $W=a+b$.

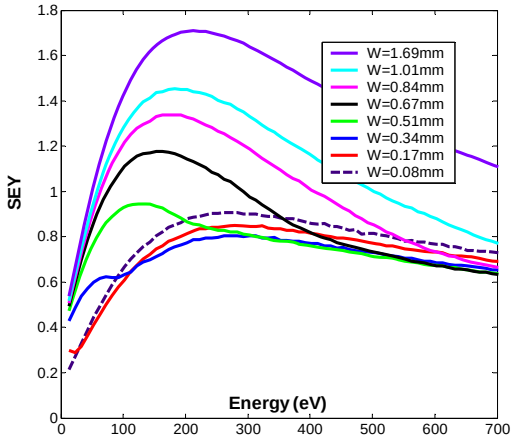

Fig. 12. Effective SEY from a rectangular surface in a dipole magnetic field. δ_{max}=1.74, E_{max}=330eV, B_0=0.2Tesla. A small *a* is used.

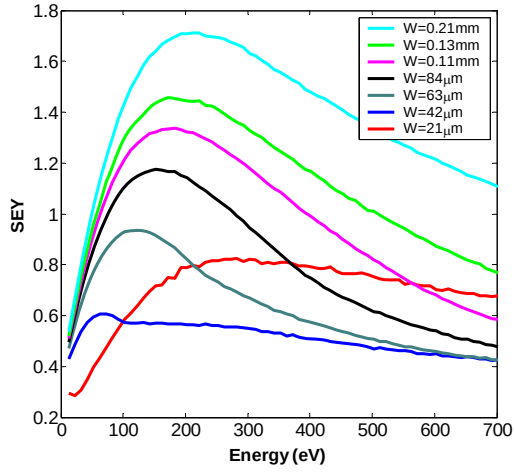

Fig. 13. Effective SEY from a rectangular surface. δ_{max}=1.74, E_{max}=330eV, B_0=1.6Tesla.

APPLICATION AND DISCUSSION

Configuration of grooved surface

In a general multipole magnet, the magnetic field can be expressed as

$$B_r^n = (-1)^{n-1} C r^{n-1} \sin n\theta, \quad (9)$$

$$B_\theta^n = C r^{n-1} \cos n\theta, \quad (10)$$

where $2n$ is the number of poles in order to excite the nth multipole, n=1 for dipole, 2 for quadrupole and so on. C is constant value for each type of magnets. In a strong magnet, electrons can drift to the chamber center only along the magnetic field lines with stronger radial field component. These field lines are close to position which satisfies

$$\sin n\theta \sim \pm 1. \quad (11)$$

These points are the middle position of magnet poles. Therefore, the grooved surface should locate near these positions to suppress the electron multipacting there,

while smooth surface can be used in other regions in order to reduce the total impedance of beam chamber.

Fig. 14 shows the transverse distribution of electron cloud in a dipole and quadrupole magnet of ILC positron damping ring. Two multipacting strips near the horizontal center are clearly visible in the dipole magnet. The width of multipacting region is only 10*mm* where the grooved surface at both bottom and top of the chamber is required. The required grooved surface is only 15% of the total surface in this case. Following the same way, the electron cloud in quadrupole, sextupole and wiggler can be reduced by replacing the smooth surface with the sawtooth and isosceles triangular surface near the magnet poles or multipacting regions.

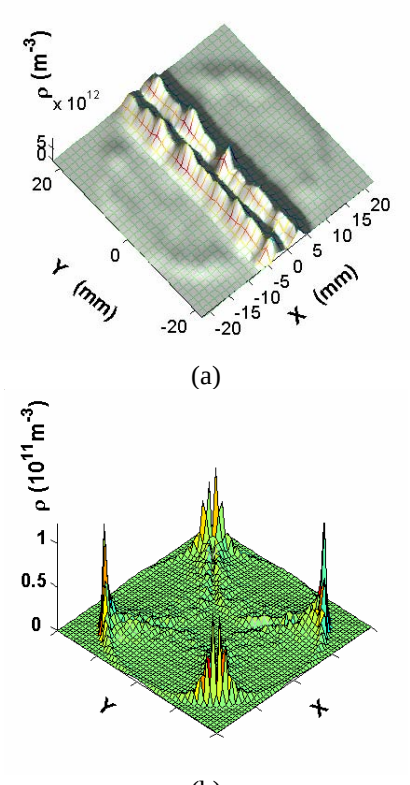

Fig. 14: Typical transverse distribution of electron cloud in the dipole and quadrupole magnet.

Enhancement of the resistive wall impedance

Due to the sharp edges on the corrugated surface, the resistive wall wake generated by a beam will be increased by a scale factor when compared to that of a flat pipe. For rectangular fins the impedance increase was calculated in Ref. [31]. Here we will calculate the enhancement factor for triangular fins shown in Fig. 8.

The energy loss induced by the electromagnetic field inside the wall in the small skin depth approximation (a so called Leontovich boundary condition [32]) is proportional to the square of the magnetic field on the metal surface. Therefore, the enhancement η of the resistive wall wake effect (both transverse and longitudinal) for the finned beam pipe, compared to a normal beam pipe, can be written as

$$\eta = \frac{\int H^2 ds}{H_0^2 W} \qquad (12)$$

where H is the magnetic field of the beam on the surface of the metal, H_0 the magnetic field in the case of a flat (non-grooved) surface, and integration follows the grooved surface over one period in a plane of constant z (the z axis points out of the page in Fig. 15). The magnetic field can be represented as $H = \hat{z} \times \nabla \varphi$, with $\hat{z}$ the unit vector in z and the magnetic potential φ satisfying the two-dimensional Laplace equation $\nabla^2 \varphi = 0$. Note that using the Laplace equation for the magnetic field is valid for frequencies ω such that $c/\omega >> W$; for example, for W~3*mm* this means $\omega \leq 2\pi \cdot 10^{11}$ Hz.

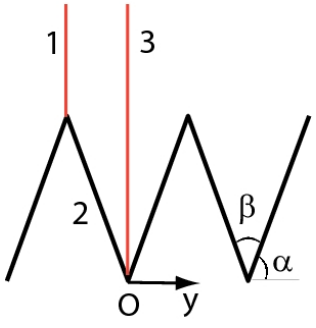

Figure 15: Triangular grooves and the region for the problem that is actually solved. This region is bounded by two vertical lines 1 and 3 and the metal surface 2; it covers half of the period of the groves. The z axis points out of the page and the origin of the coordinate system is located at the point O with the x and y axis going in the vertical and horizontal directions respectively.

Neglecting the curvature due to the pipe radius R (which is valid if R is much larger then the fin depth $W/2\tan(\beta/2)$) and using the symmetry of the problem, we actually solve the Laplace equation for the geometry shown in Fig. 15, which covers half of the period $W/2$. The boundary condition for the magnetic field **H** is that it is tangential on the surface of the metal, perpendicular to the vertical lateral boundaries and it approaches the value of H_0 far from the surface when $x \to \infty$. In terms of the potential φ this means that $\varphi = 0$ on the metal surface, $\partial\varphi/\partial n = 0$ at the vertical boundaries, and $\varphi \to H_0 x$ as $x \to \infty$.

The solution $\varphi(x, y)$ can be obtained with the help of a conformal mapping using the Schwartz-Christoffel integral [33]. We introduce the complex variables $w = \varphi + i\phi$ and $u = x + iy$, with φ being the magnetic potential, ϕ an auxiliary function and x and y the rectangular coordinates shown in Fig. 15. Omitting the

derivation, we present here the final result of the conformal map *u(w)*:

$$u = \frac{1}{\gamma}(-\zeta)^{\gamma}\,{}_2F_1(\gamma,\gamma;\gamma+1;\zeta) \tag{13}$$

$$\zeta = \frac{1}{4}e^{-w}(1+e^{w})^2 \tag{14}$$

where $\gamma = \beta/2$, and ${}_2F_1$ is the hypergeometric function. The real part of the inverse function $u^{-1}(w)$ gives the potential φ as a function of coordinates *x* and *y*. It is easy to show that the enhancement factor Eq. (1) is given by the following equation

$$\begin{aligned}\eta &= \left|\frac{1}{\pi}\int_0^1 d\zeta \frac{(dw(\zeta)/d\zeta)^2}{du(\zeta)/d\zeta}\right| \\ &= \left|\frac{1}{\pi}\int_0^1 d\zeta(\zeta-1)^{\gamma-1}\zeta^{\gamma-1}\right| = \frac{1}{\cos(\pi\gamma)}\end{aligned} \tag{15}$$

The plot of the amplification factor as a function of angle is shown in Fig. 17. For the angle $\alpha = 70^0$ the enhancement η=2.9.

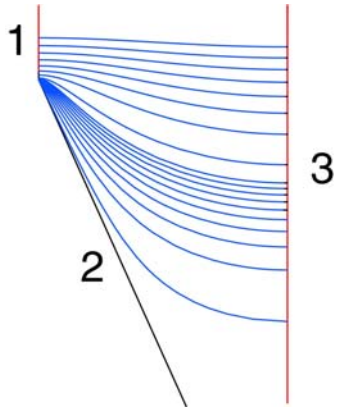

Figure 16: Magnetic field lines penetrating in a groove (a half a period of a groove is shown). The numbers correspond to the numeration in Fig. 15 with the line 2 being the metal surface of the triangular fin.

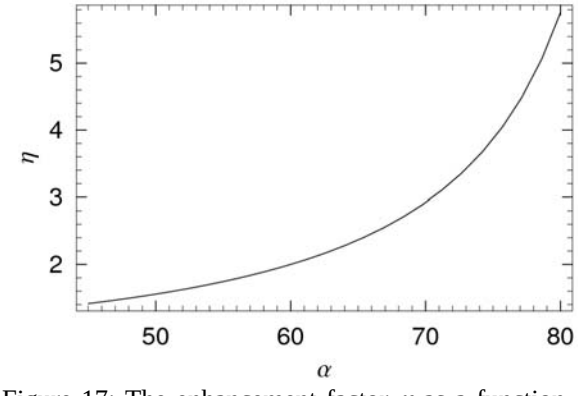

Figure 17: The enhancement factor η as a function of angle.

Although our derivation used the symmetry of the grooves shown in Fig. 8, and, strictly speaking, it is not applicable for the grooves shown in Fig. 4, we expect that the enhancement factor for both geometries should be approximately the same. The reason for this is that the increase of losses is due to the local concentration of the magnetic field near the tips of the edges of the grooves with the resulting amplification of the surface currents in those areas. This amplification effects is mostly determined by the edge angle and is rather insensitive to the detailed shape of the grooves.

Note that the enhancement of the wake will be not so dramatic if the corners of the grooves are rounded, as was shown in Ref. [31] for rectangular grooves. A rectangular grooved vacuum chamber with rounded corner cover the whole chamber surface increases the impedance approximately by a factor of 1.5[31]. If we assume the enhancement factor of 2.0 for the triangular surface with rounded tips, the increase of the impedance due to the sawtooth and isosceles triangular surface is in the dipole magnet (Fig.14a) would be 15%.

Ante-chamber will be used in the ILC to reduce the number of photons. The sawtooth surface can be applied to the photon absorber in the ante-chamber to decrease the photon reflectivity without increase of the impedance [21].

Manufacture and SEY with rounded tips

A smooth surface is required in our technique in order to trap the secondary electrons. In principle, machining is required to produce the sharp triangle and it is expensive compared to the blasting or chemical roughening. The grooved surface can be produced mechanically by rolling or extrusion with keeping small roughness along one of directions (along the beam propagation in a storage ring, for example). The grooved surface can be made by extrusions of relatively soft material, such as aluminum and copper. Copper-coated aluminum is a possible way to make a low SEY triangle surface. A new rolling-tap method is developed to make the sawtooth surface in a circular beam chamber with a length of several meters [21].

The tip of triangular is likely to be rounded by blasting or chemical roughening and a rounded tip can not reduce the SEY as expected. The effect of small round tip depends on the probability of electrons hit this tip. Fig. 18 shows a triangular surface with rounded tips. Fig. 19 shows the effective SEYs of the geometry shown in Fig. 18. The radius of rounded tip R_{tip} is 0.2*mm*. The SEYs are increased due to the rounded tips, but it is still low enough to suppress the electron multipacting. The SEYs can be further reduced by making a sharp bottom (keeping rounded tips) without changing the impedance due to its weak magnetic field there (Fig. 16). A similar SEYs can be achieved for various sizes of the triangular surface.

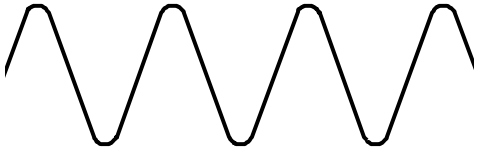

Fig. 18. Triangular groove with rounded tips

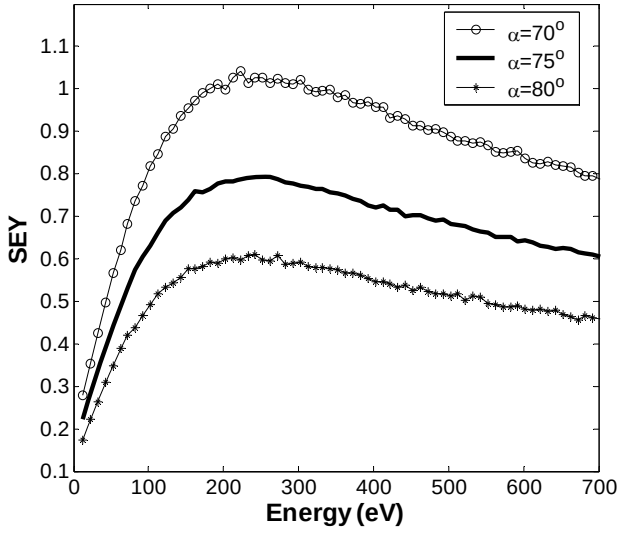

Fig. 19. Effective SEY of an isosceles triangular surface with rounded tip. δ_{max}=1.74, E_{max}=330eV, B_0=0.2Tesla, R_{tip}=0.2*mm*, *W*=4.52*mm*.

Beam effect

When a secondary electron is emitted from the grooved surface, the electric field of circulating beam can attract it into the beam chamber. A weak beam can easily attract the secondary electrons due to their low energy. Therefore, a grooved surface cannot effectively reduce the SEY with a long bunch beam like SNS and LANL-PSR. The beam's effect is negligible for a short bunch like B-factories and ILC where the bunch length is a few of millimeters, which is insignificant comparing with their bunch spacing of meters. The grooved surface also works for an intermediate bunch, such as RHIC type of beam, where there is a bunch length about 10ns and a long bunch spacing of 108ns. The electrons are swept to the pipe surface after the bunch passage and then multipacting happens. The grooved surface can kill the secondary electrons during the long bunch spacing. Note that a sawtooth surface doesn't work in field free region of KEKB positron ring where strong multipacting occurs [21]. In that case, the grooved surface effectively reduces the number of photons, however, it can't suppress the electron multipacting. As a result, the grooved surface doesn't reduce the number of electrons due to electron multipacting.

SUMMARY

The effective SEY from various grooved surface in a magnetic field has been simulated using Monte Carlo method. Both sawtooth and isosceles triangular surface can significantly reduce the effective SEY below the multipacting threshold. The suppression effect is sensitive to the slope angle α and has weak dependence on the size of the surface and the magnetic field. A larger α is more effective. The effective SEY becomes independent on the size of surface and magnetic field when W >2*mm* in a magnetic field B_0>0.2 Tesla. Such kind of surface can suppress the electron multipacting up to a δ_{max}=2.5 with α>70° and W>0.4*mm*. The suppression characters of very weak dependence on the size and magnetic field make these two surfaces work universally. Note that there is no upper limitation on *W*. Therefore, it is easy to be fabricated and it is cheap. Ideally, the suppression effect of SEY and the impedance enhancement of the isosceles triangular surface is only a function of the slope angle α.

A rectangular surface also can effectively reduce SEY with a small range of size. However, its effect is notably sensitive to the size of surface and magnetic field. The required size *W* ranges from 0.08*mm* to 0.51*mm* and from 21μm to 63 μm in a 0.2 Tesla and 1.6 Tesla magnetic fields, respectively. The sensitivity to the size and magnetic field limits the application of the rectangular surface. For example, a rectangular grooved surface is inapplicable to the wiggler magnet due to the small required size and the variation of magnetic field in the beam direction. A half *mm* scale of rectangular surface can be used in ILC dipole magnets.

In practice, rounded/smooth tips is required for the all grooved surfaces in order to reduce the impedance, especially for the triangular surfaces. A larger size of triangular surface with a small rounded tips is the best option for manufacture, suppression of SEY and reducing impedance. The impedance enhancement due to the sawtooth and isosceles triangular surface is likely small due to the small percentage of the coverage of the grooved surface. A detail study of the impedance with the realistic geometry (with rounded tips) is under the way. The sawtooth and isosceles triangular surface can suppress the electron multipacting in various magnets, such as dipole, quadrupole and wiggler.

ACKNOWLEDGMENT

The authors gratefully thank K. Bane, Y. Cai, R. E. Kirby, B. McKee, M. Pivi and A. Seryi for many useful discussions. We thank M. Pivi for introducing this problem. We also thank Y. Suetsugu at KEK for discussion about the manufacture of the grooved surfaces and for providing the valuable references.

REFERENCES

[1] CERN Yellow Report, CERN-2002-001(2002).

[2] H. Fukuma, CERN-2002-001 (2002).

[3] L. F. Wang, H. Fukuma, K. Ohmi, KEK-Report 2001-2(2001).

[4] Y.Suetsugu, et al., in Proceeding of 2001 Particle Accelerator Conference, p2180, Chicago (IEEE, Piscataway, NJ, 2001).

[5] P. McIntyre and A. Sattarov, in Proceedings of 2005 Particle Accelerator Conference, p2971, Knoxville, Tennessee, USA, 2005.

[6] L. Wang, et. al., in Proceeding of 10th European Particle Accelerator Conference, p1489, Edinburgh, UK, June 26-30, 2006.

[7] R. E. Kirby and F. K. King, Nucl. Inst. Meth. A, A469:1-12(2001).

[8] F. Le Pimpec, R. Kirby, F. King., M. Pivi, Nucl. Inst. Meth. A551, 187:199(2005).

[9] B. Henrist, N. Hilleret, C. Scheuerlein, M. Taborelli, Applied Surface Science, 172:95-102(2001).

[10] P. He, et al. in Proceeding of 9th European Particle Accelerator Conference, p1804, Lucerne, Switzerland, 2004.

[11] H. Hseuh, et al., in Proceedings of ECLOUD'04, Napa, California, April 2004, CERN-2005-1.

[12]Y. Suetsugu, et al., Nucl. Instrum. Meth. A554:92-113(2005).

[13]Y. Suetsugu, K. Kanazawa, K. Shibata and H. Hisamatsu, Nucl. Instrum. Meth. A556:399-409(2005).

[14] E. Hoyt, et al., in Proceeding of 1995 Particle Accelerator Conference, p2054, Dallas, TX, (1995).

[15] S.Y. Zhang, et al., in Proceeding of 9th European Particle Accelerator Conference, p947, Lucerne, Switzerland, 2004.

[16] J.M. Jimenez, et al., LHC-Project-Report-634 (2003).

[17] J. Kawata, K. Ohya and K. Nishimura, Journal of nuclear Materials 220-222 (1995) 997-1000.

[18] V. Baglin, et. al., in Proceeding of 7th European Particle Accelerator Conference, Vienna, Austria, 2000.

[19] G. Stupakov and M. Pivi, Stanford linear accelerator center report, SLAC-TN-04-045, SLAC(2004).

[20] A. A. Krasnov, Vacuum 73 (2004) 195.

[21] Y. Suetsugu, et al., J. Vac. Sci. Technol. A 21(1), 186 (2003).

[22] V.V. Anashin, et al., Vacuum 60 (2001) 255

[23]M. Pivi, et al., in Proceedings of 2005 Particle Accelerator Conference, p24, Knoxville, Tennessee, USA, 2005.

[24] Y. Suetsugu, private communications.

[25] M. A. Furman and G. R. Lambertson, in Proceedings of the International Workshop on Multibunch Instabilities in Future Electron and Positron Accelerators, Tsukuba, 1997 (KEK Report No. 97-17, 1997), p. 170–199.

[26] H. Seiler, J. Appl. Phys. 54, R1–R18 (1983).

[27] Robert E. Kirby and Frank K. King, "Secondary Electron Emission from Accelerator Materials," in Proceedings of the 8th ICFA Beam Dynamics Mini-Workshop on Two-Stream Instabilities, Santa Fe, 2000, http://www.aps.anl.gov/conferences/icfa/two-stream.html; R. Kirby and F. King, "Secondary Electron Emission Yields from PEP-II Accelerator Materials", SLAC Report No. SLAC-PUB-8212, 2000.

[28] L. F. Wang, et. al., Physical Review Special Topics - Accelerators and Beams, Volume 5, 124402 (2002).

[29] L. F. Wang, D. Raparia, J. Wei, and S.Y. Zhang, Physical Review Special Topics - Accelerators and Beams, Volume 7, issue 3, 34401 (2004).

[30] J. M. Jimenez, et al, CERN-2002-001, 2002.

[31] K. L.F. Bane and G. Stupakov, Stanford Linear Accelerator Center report, SLAC-PUB-11677 (2006). Also in Proceeding of 10th European Particle Accelerator Conference, p2961, Edinburgh, UK, June 26-30, 2006.

[32] L. D. Landau and E. M. Lifshitz, Electrodynamics of Continuous Media, vol. 8 of Course of Theoretical Physics (Pergamon, London, 1960), 2nd ed., (Translated from the Russian).

[33] C. Ruel V and J. W. Brown, Complex variables and applications (McGraw-Hill, 1989), 5th ed.